Computational Assessment of Drag Behavior for Spiked Light Assault Missile.

Ahmed Fayez[1*], OSAMA KAMAL[2], M. Ahmed[3]

[1] M.Sc. Student, Aerospace Engineering Department, Military Technical College, Egypt
[2] Ph.D., Senior lecturer at Aerospace Engineering Department, Military Technical College, Egypt
[3] Professor, Aerospace Engineering Department, Military Technical College, Egypt

*E-mail: ahmedfayez305@gmail.com

Abstract. This paper presents a comprehensive numerical analysis of the aerodynamic behaviour of a spiked light missile designed for supersonic flight. The study focuses on the impact of a forebody-mounted spike on drag reduction and shock wave mitigation at speeds up to Mach 2.5. Utilizing a 3D, double-precision, pressure-based solver and the Shear Stress Transport (SST) k-ω turbulence model, the simulations accurately capture boundary layer separation and shock-wave interactions, essential for high-speed aerodynamic assessments. The computational domain is carefully defined to encompass the detached shock wave system generated by the missile's blunt nose and spike, ensuring that all relevant flow phenomena are analysed. The results indicate that the spike design significantly alters the pressure distribution on the missile's forebody, leading to a notable reduction in drag. The findings underscore the importance of aerodynamic drag reduction techniques in improving the performance and fuel efficiency of high-speed vehicles, contributing valuable insights to the field of aerospace engineering.

1. Introduction

The study of aerodynamic drag reduction techniques is of paramount importance in supersonic flight due to its direct impact on fuel efficiency, speed, and overall performance of high-speed vehicles. The formation of strong shock waves and flow separation significantly contributes to aerodynamic drag, necessitating the development of various drag reduction methods. These techniques include nose modifications, energy deposition, active and passive flow control, and the implementation of spike attachments [1]. Among these methods, the use of a spike mounted on the forebody of a blunt-nosed vehicle has proven to be one of the most effective techniques for reducing aerodynamic drag and mitigating shock wave intensity [2].

A spike is an elongated structure affixed to the leading edge of a vehicle's forebody, designed to alter shock wave patterns and improve aerodynamic efficiency. When introduced in supersonic flow, the spike generates a detached shock wave upstream, creating a recirculating flow region that reduces pressure intensity on the vehicle forebody, thereby lowering both drag and heat transfer rates [3]. Studies have shown that spike-induced flow restructuring significantly enhances aerodynamic performance by altering shock interactions and boundary layer behaviour [4,5].

Previous investigations have extensively analysed the aerodynamic benefits of spiked bodies in supersonic and hypersonic regimes. Researchers have explored various spike geometries, including conical, hemispherical, and flat-tip spikes, to evaluate their impact on drag reduction and flow stability [6]. Experimental and computational studies indicate that spike length, tip shape, and diameter ratio play critical roles in determining aerodynamic efficiency [7]. By modifying the shock wave pattern, spikes also help in reducing aerodynamic heating, which is a critical concern for supersonic missiles. The recirculating flow zone created by the spike acts as a buffer, reducing the heat transfer to the missile's surface [8]. While spikes offer significant aerodynamic benefits in supersonic conditions, their effectiveness can vary based on the specific design and flight parameters. The choice of spike shape, length, and integration with the missile body must be carefully considered to maximize performance

while minimizing potential drawbacks such as increased pressure fluctuations or impaired performance in transonic conditions [9]. The adoption of Computational Fluid Dynamics (CFD) for aerodynamic analysis provides significant advantages over experimental testing, including cost-effectiveness, flexibility in evaluating different design configurations, and detailed insights into flow behaviour under varying conditions [10]. CFD enables the visualization of complex shock structures, pressure distributions, and aerodynamic forces, facilitating a comprehensive understanding of spike modifications on aerodynamic performance [11]. Recent advancements in high-fidelity turbulence modelling and grid refinement techniques have further improved the predictive accuracy of CFD simulations, making them an indispensable tool for supersonic flow investigations [12,13]. By leveraging numerical simulations, this study aims to optimize spike configurations for enhanced aerodynamic performance in supersonic flight conditions [14,15].

The present study addresses a light assault missile which forebody is made blunt that is expected to yield unacceptably high drag. To minimize drag, a spike is added to the forebody design. This study is sought to explore drag behavior of the spiked missile. The remainder of the paper is organized as follow.

The next section demonstrates the details of case study and research methodology. The section that follows discusses the results of the present research. the paper finalizes by high lighting the key findings and conclusions.

2. Case Study and Methodology

The missile geometry, as shown in Figures 1, consists of a cylindrical body with three stabilizing fins at the rear. A spike mounted on the large blunt forebody is aimed to reduce aerodynamic drag and shockwave intensity. The spike, extending from the blunt nose, is expected to generate a leading detached shock and a recirculating flow region, thereby influencing the overall aerodynamic behaviour. The total missile length is 26.5 times the body diameter (d), while the maximum forebody diameter is 1.42d.

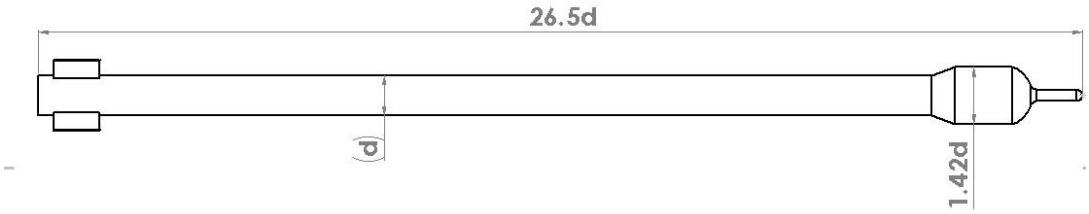

Figure 1. geometry of case study Missile.

The analysis will focus on drag coefficient (C_D), pressure distribution, and shock wave formation. Focus is made on the rang of flight Mach number from 0.5 to 2.5 at sea level conditions and zero incidence. Contribution of each airframe element in drag is addressed as well.

Previous studies have demonstrated that the size of the computational domain significantly affects the accuracy of computational fluid dynamics (CFD) simulations [16].

To ensure accurate numerical simulations, an appropriate computational domain is designed to capture all relevant flow phenomena around the missile. The chosen domain must be sufficiently large to accommodate the detached shock wave system generated by the blunt nose and spike while also allowing for analysis for the entire Mach number range.

The computational domain for this study has been defined as a symmetric hemispherical region, as illustrated in Figure 1. The domain extends 20d upstream, 107d in the lateral direction (domain diameter), and 18d downstream.

Figure 2 provides a detailed schematic of the computational domain, illustrating the spatial extents and ensuring clarity in numerical setup considerations.

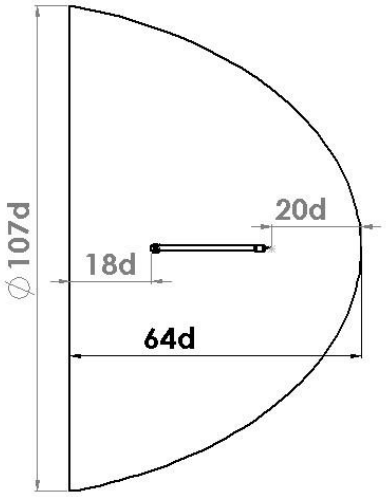

Figure 2. Computational domain.

The computational domain is defined with a pressure far-field boundary condition at the inlet to replicate undisturbed free-stream conditions, while a pressure-outlet condition is imposed at the domain exit to maintain ambient static pressure and prevent nonphysical pressure build-up. The missile surface is modelled as a no-slip wall to accurately simulate viscous effects, boundary layer development, and shear stress distribution. The working fluid is assumed to be dry air modelled as an ideal gas under standard sea-level atmospheric conditions. A 3D, double-precision, pressure-based solver is employed to ensure numerical stability and accurate drag prediction. Shear Stress Transport (SST) k-ω turbulence model is selected for its capability in capturing boundary layer separation and shock-wave interactions, balancing near-wall accuracy with freestream robustness. Second-order upwind schemes are used for convective terms to enhance accuracy and reduce numerical diffusion. Simulations are conducted until all residuals drop below 10^{-6} and the drag coefficient stabilizes, confirming solution convergence.
The computational grid is generated using an unstructured mesh to accurately capture the complex flow features, particularly around the shock waves, boundary layers, and separation regions. Additional mesh refinement is applied at regions of high flow gradients, such as the spike tip, shock interaction zones, and the missile base, to enhance resolution and accuracy.

To ensure grid-independent results, a mesh sensitivity study is conducted at Mach 2 and zero incidence by varying the total number of computational cells and observing changes in the drag coefficient.

Multiple mesh resolutions are tested as shown in Table 1. The results show that at 3,846,724 and 4,012,759 cells, the changes in drag coefficient are below 1%. Therefore, a mesh size of 3,846,724 cells is selected for all subsequent simulations to balance accuracy and computational efficiency.

Table 1. Mesh Sensitivity Analysis Results.

Trial no.	Number of cells	C_D	Change (%)
1	299664	1.8635	————
2	1021430	1.7592	5.5965
3	1754623	1.6763	4.7125
4	3000000	1.6405	2.1362
5	3846724	1.6192	1.3008
6	4012759	1.6078	0.7

3. Results and discussions

3.1 Validation of CFD Model

This section presents the validation of proposed CFD model. This is sought by computing aerodynamic characteristics of a canard-controlled missile with fixed and free-rolling tail fins at various Mach numbers. The experimental data from the wind-tunnel investigation [17] are compared with our CFD simulations results to confirm the accuracy of the numerical model. Figure 3 represents the missile used in the CFD simulations. The model clearly illustrates critical geometric features, including the pointed nose cone, cylindrical body, and stabilizing fins, ensuring an accurate replication of the experimental test article.

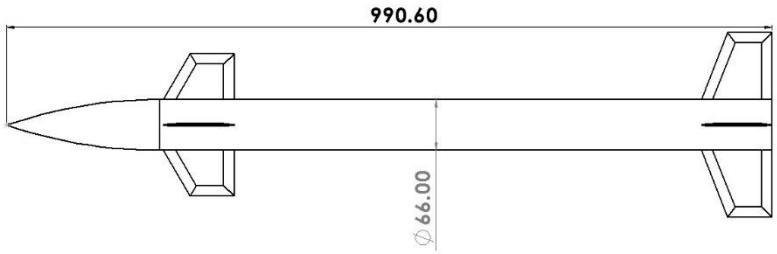

Figure 3. Validation case Missile [17].

To replicate the experimental conditions accurately, a detailed CFD model is developed, ensuring consistency with the missile geometry, Mach number range, and boundary conditions, including sea-level atmospheric conditions. Following model development, CFD simulations were executed to generate lift coefficient (C_L) and drag coefficient (C_D) values at the same angle of attack (AoA) points recorded experimentally. Maintaining identical operating conditions to ensure a direct comparison with wind-tunnel data. The resulting aerodynamic coefficients from the numerical simulations were systematically compared to the experimental data by plotting C_L against C_D, enabling the assessment of trends and absolute values. The final comparison between the experimental and simulated results is illustrated in the following figures, demonstrating the effectiveness of the numerical approach in capturing the key aerodynamic characteristics of the missile.

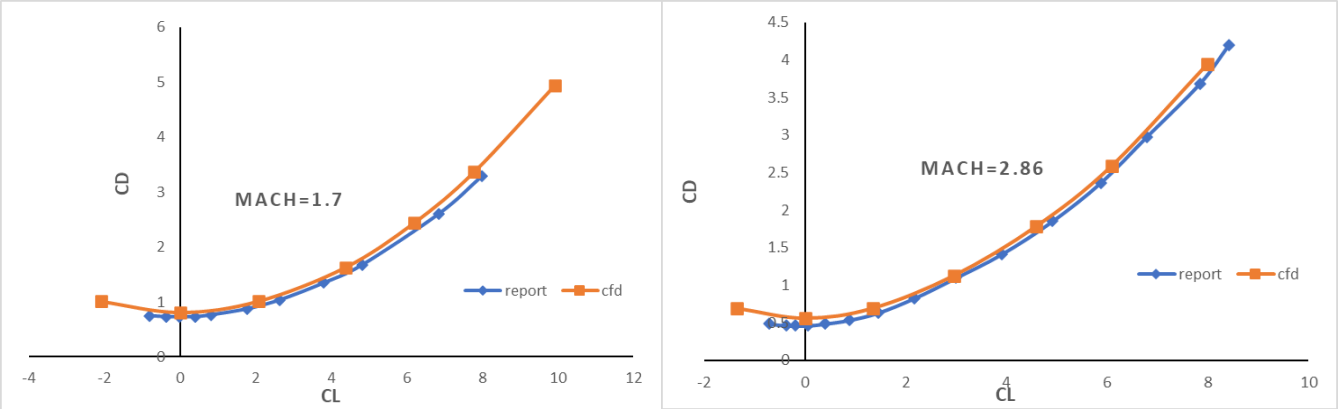

Figure 4. Lift Coefficient vs Drag Coefficient at Mach 1.7 and Mach 2.86.

Figure 4 presents Lift Coefficient the (C_L) vs Drag Coefficient (C_D) at Mach 1.7 and Mach 2.86, with both experimental data (represented by blue dots) and the CFD results (represented by orange squares) showing similar trends. This small error is due to support clamp at the base, thereby validating the aerodynamic performance at this Mach number. The validation process demonstrates that the CFD model accurately reproduces the aerodynamic behaviour observed in report. Key aerodynamic parameters, such as the lift and drag coefficients, exhibit trends and absolute values that closely match the experimental data. This successful validation establishes confidence in the CFD model predictive capabilities for further aerodynamic analysis of case study missile.

3.2. drag behavior for case study missile

The drag coefficient (C_D) variation with Mach number at zero incidence exhibits distinct trends characteristic of subsonic, transonic and supersonic flow regimes as illustrated in figure 5.

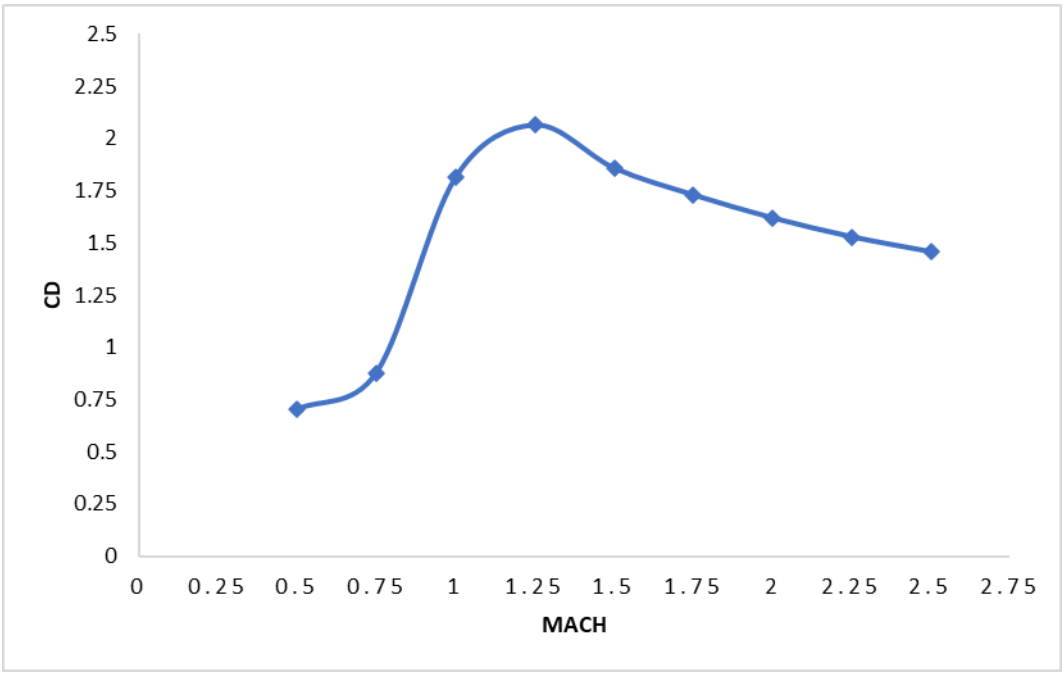

Figure 5. Mach number vs drag coefficient at zero incidence for case study missile.

At subsonic speeds the drag coefficient remains relatively low with only a slight increase as the flow accelerates toward the transonic regime. The critical value of Mach number assumed at around

0.6 while drag divergence may take place at Mach 0.75. Around Mach 0.8–1.0, a sharp rise in C_D is observed, corresponding to the formation of shock waves and the onset of flow separation—a well-known phenomenon in transonic aerodynamics. As the flow transitions to supersonic speeds, the drag coefficient reaches a peak near Mach 1.2–1.3, attributable to the strong bow shock formation ahead of the missile body, which significantly increases pressure drag. Beyond this point, as the Mach number increases further, C_D gradually decreases, indicating a reduction in shock strength. This trend continues up to Mach 2.5, where C_D tends to stabilize at a lower value.

3.3. Drag component for case study missile

The total drag coefficient (C_D) of a missile is composed of contributions from various components, including the spike, head, cylinder, base, and fins. Table 2 presents, the percentage contribution for each component at different Mach numbers to the total drag coefficient.

To analyse the relative impact of each component, the percentage contribution to the total drag coefficient is calculated as:

$$\% \textbf{ Component Contribution} = \left(\frac{C_{D_{Component}}}{C_{D_{Total}}}\right) * 100.$$

Table 2. Component Contribution to Total Drag Coefficient.

Mach	$C_{D_{spike}}(\%)$		$C_{D_{head}}(\%)$		$C_{D_{cylinder}}(\%)$		$C_{D_{base}}(\%)$		$C_{D_{fins}}(\%)$	
	C_{D_p}	C_{D_v}	C_{D_p}	C_{D_v}	C_{D_p}	C_{D_v}	C_{D_p}	C_{D_v}	C_{D_p}	C_{D_v}
0.5	13.33	0.34	22.05	4.42	0.11	27.50	21.13	0	9.75	1.38
0.75	12.06	0.20	42.31	1.28	0.13	18.43	17.07	0	7.74	0.86
1	6.54	0	67.24	1.77	0.09	7.94	11.72	0	4.34	0.37
1.25	6.48	0	68.41	1.29	0.09	7.17	11.68	0	4.39	0.39
1.5	6.29	0	66.82	1.38	0.10	7.89	12.04	0	5.04	0.45
1.75	6.61	0	66.33	1.35	0.10	8.11	11.64	0	5.36	0.49
2	6.99	0	66.20	1.31	0.11	8.18	11.10	0	5.63	0.49
2.25	7.47	0	65.67	1.27	0.11	8.38	10.58	0	6.00	0.53
2.5	7.61	0	66.83	1.23	0.10	8.09	9.73	0	5.94	0.47

The analysis indicates that the spike accounts for approximately 5–10% of the total drag across all Mach numbers, confirming its primary function in modifying shock structures to reduce overall aerodynamic resistance rather than acting as a major source of drag. The head, however, dominates the drag characteristics—its contribution peaks at 69.0% at Mach 1.0 due to strong local shock wave formation. Although its relative contribution decreases beyond Mach 1.25, it remains the principal drag-producing element. The cylindrical body contributes a modest 6–11% of the total drag, a consistency that is expected given that it primarily experiences skin friction rather than shock-induced pressure drags. Meanwhile, the base drag exhibits a decreasing trend with increasing Mach number, declining from 21.1% at Mach 1.0 to 9.7% at Mach 2.5, which aligns with the reduction in wake effects at higher supersonic speeds. Lastly, the fins contribute between 4–7% to the overall drag, playing a minor yet consistent role throughout the examined Mach range.

3.4. Flow field features

The numerical simulation of the missile flow field provides critical insights into the flow behaviour at different speeds. The computational results highlight key flow structures, including the formation of a bow shockwave, boundary layer development, recirculation zones, and flow separation patterns. The following analysis describes the major flow features observed in the simulation results.

Figure 6 presents the absolute pressure contour around the missile at different speed, illustrating the formation of a strong bow shockwave at the tip of the spike. This detached shock forms due to the supersonic freestream encountering the spike tip, causing a sudden increase in pressure. The shockwave significantly alters the downstream flow behaviour by creating a region of high-pressure stagnation just ahead of the missile body. This precompression effect reduces the intensity of the subsequent shock interactions on the main missile body. The colour gradient in the pressure contour also highlights expansion and recompression zones along the missile, where the pressure variations contribute to the complex aerodynamic load distribution.

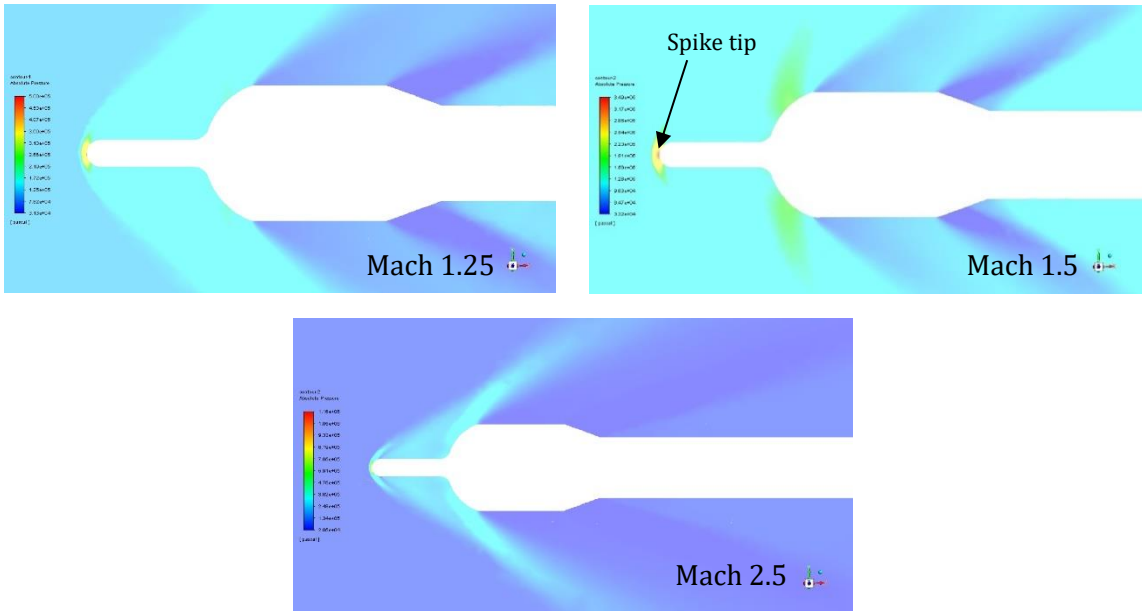

Figure 6. Absolute pressure contour around the missile indifferent Mach.

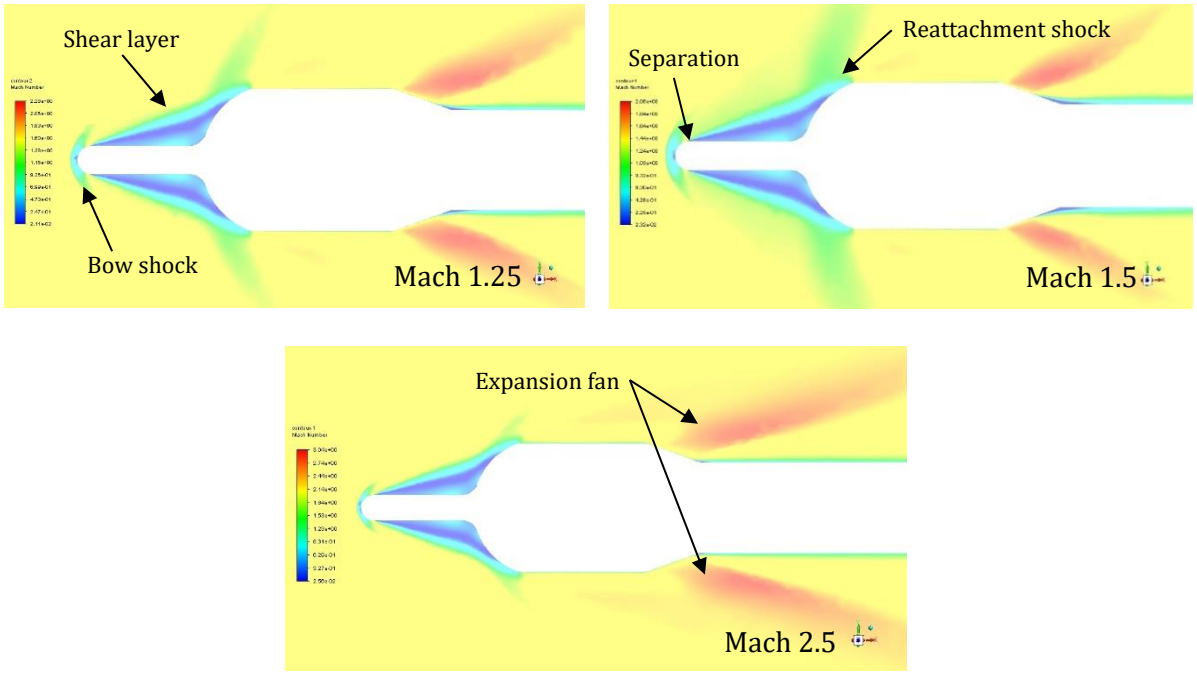

Figure 7. Mach number contour around the missile at different Mach.

Figure 7 displays the Mach number contour at different speed, which captures the distribution of flow velocities throughout the domain. The high-speed supersonic flow around the missile undergoes

significant deceleration across the bow shockwave, as indicated by the transition from red (higher Mach values) to blue (lower Mach values). Immediately downstream of the spike tip the boundary layer detaches forming a recirculation region. characterized by locally subsonic flow and low pressure due to the interaction of expansion waves and adverse pressure gradients. The Mach number contour also reveals the boundary layer development along the missile surface, where the flow velocity gradually decreases due to viscous effects. This boundary layer remains largely attached over the forebody but begins to thicken towards the aft section, contributing to wake formation and potential flow separation.

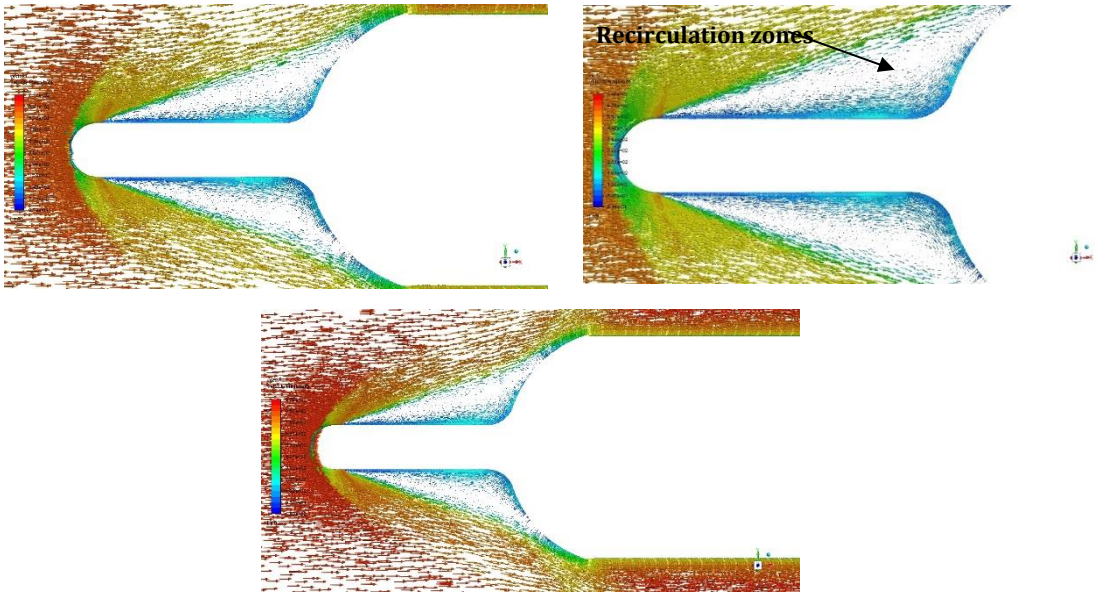

Figure 8. velocity vector field around the missile at different Mach.

Figure 8 illustrates the velocity vector field, offering a detailed visualization of flow direction and velocity magnitude. This figure captures the formation of recirculation zones immediately behind the spike, were flow reverses direction due to local adverse pressure gradients. These zones act as flow buffers, mitigating direct aerodynamic loading on the missile body. Additionally, the velocity vectors indicate regions of flow reattachment, where the separated shear layer from the spike recombines with the freestream. The interaction between the separated and attached flow plays a crucial role in modifying the missile drag characteristics. Notably, the aft section of the missile exhibits regions of wake turbulence and flow separation, as depicted by the dispersed velocity vectors, which contribute to the overall aerodynamic performance.

4. conclusion

This study effectively demonstrates the aerodynamic advantages of a forebody-mounted spike on a light missile designed for supersonic flight, revealing that the spike significantly reduces aerodynamic drag and mitigates shock wave intensity, which are crucial for enhancing missile performance. The numerical simulations conducted using Computational Fluid Dynamics (CFD) confirmed that the spike design alters the shock wave pattern, creating a detached shock wave and a recirculating flow region that positively influences the missile's aerodynamic behaviour, while also modifying the pressure distribution on the forebody, leading to a notable reduction in drag. The validation of the CFD model against experimental data establishes its reliability in predicting aerodynamic characteristics, providing a solid foundation for future investigations into spiked missile configurations. Overall, this research contributes valuable insights into drag reduction techniques, highlighting the importance of spike design in optimizing the performance of high-speed vehicles, with future work potentially exploring additional modifications to further enhance aerodynamic efficiency in supersonic.

5.References

[1] Smith, J., Brown, P., and Lee, T., 2022, *Review of Wave Drag Reduction Techniques: Advances in Active, Passive, and Hybrid Flow Control*, Proceedings of the Institution of Mechanical Engineers, Part G: Journal of Aerospace Engineering, Vol. **236**, No. 4, pp. 785–801.

[2] Johnson, M., and Wang, H., 2024, *Mechanism of Active Flow Control Using a Novel Spike Aerodome*, Physics of Fluids, Vol. **36**, Article 012345.

[3] Martinez, R., Kim, S., and Lopez, D., 2024, *Aero-Spike and Aero-Disk Effects on Wave Drag Reduction of Blunt Bodies in Supersonic Flow*, Aircraft Engineering and Aerospace Technology, Vol. **96**, No. 2, pp. 189–204.

[4] Thompson, B., and Zhao, Y., 2018, *Drag Reduction and Aerodynamic Shape Optimization for Spike-Disk Configurations in Supersonic Flows*, AIAA Journal, Vol. **56**, No. 8, pp. 3120–3135.

[5] Carter, L., and Nguyen, P., 2021, *Shock Wave Interaction and Boundary Layer Effects on Spiked Blunt Bodies, Journal of Fluid Mechanics*, Vol. **915**, Article A13.

[6] Wilson, E., Hernandez, J., and Patel, A., 2023, *Numerical and Experimental Analysis of Supersonic Flow Over Blunt Bodies with Spikes*, Acta Astronautica, Vol. **199**, pp. 20–35.

[7] Green, M., and Choi, K., 2023, *Optimization of Nose Spike Parameters for Supersonic Vehicles*, Aerospace Science and Technology, Vol. **128**, Article 107146.

[8] Anbarasan, R., Kumar, P., and Rajendran, S., 2023, *Numerical Analysis and Design Optimization of Bluff Body Using Spike*, International Journal of Mechanical Sciences, Vol. **195**, Article 106241.

[9] Milicev, D., 2022, *Numerical Analysis and Design Optimization of Bluff Body Using Spike*, Journal of Aerospace Engineering, Vol. **37**, No. 2, pp. 150–165.

[10] Kim, H., and Sanchez, F., 2023, *High-Order Accurate Numerical Simulation of Supersonic Flow*, Fluids, Vol. **7**, Article 385.

[11] Foster, B., Nakamura, Y., and Silva, T., 2021, *Computational Investigation of Heat Transfer Reduction in Spiked Bodies*, International Journal of Heat and Fluid Flow, Vol. **82**, Article 108561.

[12] Richards, C., and Bellamy, S., 2022, *Advances in High-Fidelity CFD Modelling for Supersonic and Hypersonic Flows*, Computational Mechanics, Vol. 69, No. **5**, pp. 1031–1048.

[13] Edwards, K., Li, J., and Reynolds, P., 2023, *Grid Refinement and Turbulence Modeling in Supersonic Flow Simulations*, Journal of Computational Physics, Vol. **475**, Article 111748.

[14] Gordon, R., and Fischer, L., 2024, *Some Effects of Domain Size and Boundary Conditions on the Accuracy of Airfoil Simulations*, Journal of Aerospace Engineering, Vol. **38**, No. 1, Article 04023015.

[15] Turner, J., Khan, Y., and Douglas, E., 2023, *Multi-Objective Optimization of Blunt-Body Forebody Configurations Using CFD, AIAA Journal*, Vol. **61**, No. 3, pp. 812–828.

[16] Davis, P., and Zhao, X., 2021, *Wind-Resistant Design of Tall Buildings: Impact of Computational Domain Size on CFD Predictions*, Journal of Wind Engineering and Industrial Aerodynamics, Vol. **214**, Article 104710.

[17] NASA Technical Reports Server (NTRS), 1978, *Wind-Tunnel Investigation at Supersonic Speeds of a Canard-Controlled Missile with Fin*, (Washington, DC: NASA).